applied sciences

MDPI

Article

Cu Nano-Roses Self-Assembly from *Allium cepa*, L., Pyrolysis by Green Synthesis of C Nanostructures

Paola De Padova [1,2,*], Amanda Generosi [1], Barbara Paci [1], Bruno Olivieri [3], Carlo Ottaviani [1], Claudio Quaresima [1], Lorenza Suber [4], Fabio Di Pietrantonio [5], Giancarlo Della Ventura [2,6], Luciano Pilloni [7], S Supriya [8] and Gurumurthy Hegde [8]

1 CNR-ISM, via del Fosso del Cavaliere 100, 00133 Rome, Italy; amanda.generosi@artov.ism.cnr.it (A.G.); barbara.paci@ism.cnr.it (B.P.); carlo.ottaviani@ism.cnr.it (C.O.); claudio.quaresima@ism.cnr.it (C.Q.)
2 INFN-Laboratori Nazionali di Frascati, Via Enrico Fermi Frascati 40, 00044 Rome, Italy; giancarlo.dellaventura@uniroma3.it
3 CNR-ISAC, via del Fosso del Cavaliere 100, 00133 Rome, Italy; b.olivieri@isac.cnr.it
4 CNR-ISM, via Salaria Km 29300, Monterotondo Stazione, 00015 Rome, Italy; lorenza.suber@ism.cnr.it
5 CNR-IMM, via del Fosso del Cavaliere 100, 00133 Rome, Italy; fabio.dipietrantonio@artov.imm.cnr.it
6 Science Department, University of Roma Tre, Largo San Leonardo Murialdo 1, 00146 Rome, Italy
7 ENEA-Casaccia, via Anguillarese S. Maria di Galeria 301, 00123 Rome, Italy; luciano.pilloni@enea.it
8 Centre for Nano-materials & Displays, B. M. S. College of Engineering, Bull Temple Road, Basavanagudi, Bengaluru, Karnataka 560 019, India; supriyas@bmsce.ac.in (S.S.); hegde@bmsce.ac.in (G.H.)
* Correspondence: depadova@ism.cnr.it or paola.depadova@ism.cnr.it; Tel.: +39-06-45488144

Received: 16 April 2020; Accepted: 27 May 2020; Published: 30 May 2020

Abstract: Carbon nanostructures are achieved by bio-waste *Allium cepa*, L., (onion vulgaris) peels through pyrolysis at 900 °C. They contain dispersed elements derived by their bio-precursors, like Mg, Ca, S, Na, K, and Cu. Here, we report the self-assembly of new Cu flower-shaped nanostructures organized as nano-roses. Remarkably, the nano-roses show rolled-up petals of Cu^0 with a high chemical stability in air, exhibiting an intrinsic pure Cu crystalline phase. This suggests the exceptional potentiality to synthesize Cu^0 nanostructures with novel physical/chemical properties. The size, morphology, and chemical composition were obtained by a combination of high-resolution scanning electron microscopy, energy dispersive X-ray spectroscopy, energy dispersive X-ray diffraction, and Raman spectroscopy.

Keywords: *Allium cepa*, L., pyrolysis; green carbon nanostructures; Cu metallic nano-roses; SEM/EDS; ED-XRD; Raman spectroscopy

1. Introduction

With the fast development of nanotechnology in the last decades, the realm of nanostructures has unveiled all its beauty, giving unimaginable quantum systems, spanning all fields of physics, chemistry, and biology.

The autonomous ordering and self-assembly of atoms and molecules on atomically well-defined surfaces [1], two dimensional (2D) elemental materials such as graphene [2], silicene [3] and all those 2D beyond graphene [4–6], including van der Waals 2D heterostructures [7], transition metal dichalcogenides [8], perovskite systems [9,10] and bio-polydopamine composite materials [11] are only a small part of this, inaccessible to naked eye, extraordinary world.

The close conjugation between the atomic and nanoscopic scale of materials and their physical properties, mainly derived from the 3D, 2D, 1D, or 0D quantum size confinement [12–14], directly takes us into the mechanics applied to nanoscience and its complexity [15,16].

So far, the world of chemistry and biology has been able to strongly embrace that of physics, revealing unexpected structural, electronic, and catalytic properties of nanostructured materials that have ubiquitously flowed into the daily life, through devices and sensors.

To date, cupric oxide (CuO) has been diffusively studied thanks to its great potential applications in various fields, such as catalysis [17], solar cells [18], optical and photoconductive response [19]. It could be used, also, for its field emission properties [20], being a p-type semiconductor with a narrow band gap of 1.2 eV. One of the CuO fascinating features is its ability to form nanostructures that include many shapes, such as flower-like structures composed of hierarchical 2D nanosheets and spherical architectures. They are constituted of ultrathin nanowalls, of about 10 nm in thickness [21,22], or large honeycombs assembly on copper foils [23]. In the context of gas sensing, these CuO flower-like nanostructures are applied as electrode sensors capable of having a high non-enzymatic electrocatalytic activity for hydrogen peroxide detection [24,25].

To produce these extraordinary flower-like CuO nanostructures, chemical methods were typically used [21–25] with copper mainly treated in alkaline conditions by persulfate [21–25]. In these studies, the (-111) X-ray diffraction (XRD) reflection at $2\theta = 35.744°$ [21,24,25] and the Raman peak at 295 cm^{-1} [26] were utilized to identify the run products.

CuS nanoparticle clusters and sponge-like structures of nanoflakes were also synthesized by the chemical method by using copper chloride and thioacetamide as reagents [27,28]. These CuS were studied by scanning electron microscopy (SEM), XRD, and Raman spectroscopy to characterize their nanostructure morphology. In particular, XRD peaks specific to the hexagonal CuS structure [27] and the sharp Raman peak at 473 cm^{-1} assigned to the S-S stretching mode of S_2 ions at the 4e sites [27–30] were used for featuring the obtained compound.

Peculiar copper sulphide nanostructures, such as spheres and nanotubes, were successfully synthesized, by using a microwave-assisted solvothermal method on Cu complexes [29]. Indeed, pure CuS (hcp) with flower-like, spherical hollows and tubular structures were obtained by means of $CuCl_2 \bullet 2H_2O$ and CH_3CSNH_2 dissolved in ethylene glycol, by varying the pH by the addition of NaOH [30]. An interesting and promising application of CuS metal sulphide involves its use as anode material in lithium ion batteries [31].

Interestingly, hybrid organic–inorganic nanoflowers were accidently discovered by adding copper sulphate ($CuSO_4$) to phosphate-buffered saline solutions, containing 0.1 mg/mL bovine serum albumin at pH 7.4 and 25 °C [32]. A few days after, a precipitate appeared containing porous flower-like structures. This was the first example of a hybrid nanoflower made of both organic materials (in the form of proteins) and inorganic materials, i.e., copper (II) phosphate [32]. As further observed in [32], when an enzyme is used as the protein component, the nanoflowers showed enhanced catalytic activity, stability, and durability compared with free enzymes and other immobilization systems. These important results are probably due to either the large nanoflower surface-to-volume ratio or to the cooperative effects between the immobilized laccase molecules used and their interactions with copper (II) ions in the nanoflowers [32].

It has been known since a long time that carbon (C) provides an excellent variety of nanostructured systems, such as the C_{60} [33], C_{70} [34], C_{76} [35,36], nanotubes [37], and, last but not least, the abovementioned graphene sheet [38], occupying a dominant role either for fundamental or applied physics.

The present work is part of an ongoing study on C nanostructures synthesized by green pyrolysis at different temperatures (500, 700, and 900 °C). The main purpose of this investigation was twofold: (i) The exploitation of metallic crystalline nanostructures derived from the impurities present in red onion peels and obtained after their annealing [39,40]; and (ii) the possible application of these porous C nanostructures as sensors for toxic gases.

We obtained pure metallic nanocrystalline Cu agglomeration in C powders during green bio-waste pyrolysis from the peels of red onion [40], *Allium cepa*, L., [41]. In particular, the Cu nanostructures were

found only on the samples pyrolyzed at the highest temperature (900 °C) and not on those obtained at 500 and 700 °C (not further described here).

The aim of the present manuscript is to report the discovery of a new Cu nanostructure coined here as Cu nano-rose, due to the particular characteristic exhibited by its layers, which are spirally rolled-up like the petals of a rose.

High-resolution scanning electron microscopy (HR-SEM), energy dispersive X-ray spectroscopy (EDS), energy dispersive X-ray diffraction (ED-XRD) and Raman spectroscopy were used to exploit the morphology, chemical, and structural properties of this new arrangement of copper.

2. Materials and Methods

2.1. Sample Preparation

Carbon nanostructures were produced from the peels of *Allium cepa*, L., [41], originating from the south of India [40]. The synthesis process is considered as green for two reasons: the first related to bio-waste recycling and the second to the absence of chemical reagents. The peels were manually separated from the waste, carefully cleaned with distilled water, dried in air, and then heated in the oven at a temperature of 80 °C. Subsequently, they were crushed, reduced to powder, and selected with the use of a sieve to a size of a few tens of microns. The micrometric powder was thus pyrolyzed inside a quartz crucible at the temperature of 900 °C in an inert nitrogen atmosphere [40]. The presence of metals in fresh red onion, for safety reasons, is usually determined by means of ICPM (inductively coupled plasma mass) spectrometry [39]. We did not check directly the starting materials for our experiments. Data from the literature, however, reveal the systematic presence of several elements, including copper [39], within *Allium cepa*, L., [41] from the same provenance and type as the samples that we used for our pyrolysis.

2.2. SEM Measurements

SEM measurements on C nanostructures were carried out by using two Zeiss systems: (1) FEG-SEM, LEO 1530 (Oberkochen-Germany), equipped with an in-lens secondary electrons detector (SE), a Centaurus back scattered electron (BSE) detector, and an EDS X-ACT (detector of 10 mm^2) Oxford with an AZTEC software microanalysis system at ENEA-Casaccia, S. Maria di Galeria Rome, Italy; and (2) a Gemini 300 FE-SEM (field emission SEM), equipped with two detectors for secondary electrons, a BSE detector with five sectors, and an EDS Bruker system (detector of 60 mm^2) at LIME, Science Department, University of Roma Tre. For all experiments, we used the C powder provided by the Centre for Nano-materials & Displays, B. M. S. College of Engineering, India, lying on freshly deposited Au films on Si slabs.

2.3. Energy Dispersive XRD Measurements

ED-XRD measurements were performed in room conditions in reflection mode $\theta i = \theta r$ using the white Bremsstrahlung X-ray radiation ranging up to 50 KeV produced by a W-anode X-ray tube on a customized ED spectrometer (at CNR-ISM Rome, Italy) [42]. The detection is achieved by a cooled Ge solid state detector (SSD), probing both the incoming photons and their energy. In ED mode, there is an intrinsic reduced q-resolution of the exchanged momentum, due to the contribution of the SSD energy resolution, resulting in enlarging of the diffraction peaks, but, on the other hand, an enormous increase of the dynamic signal-to-noise ratio, with respect to the θ-2θ Bragg-Brentano geometry of conventional XRD apparatus.

2.4. Raman Spectroscopy

Raman spectra were collected with a Renishaw In-Via spectrometer, equipped with a 457-nm laser beam in standard confocal mode (at CNR-ISM Rome, Italy). The best experimental setup was obtained by combining a 2400 lines/mm grid with 100× optical magnification. The accumulation Raman spectra

was 50 with a single spectrum acquisition time of 168 s. The energy resolution was 1 cm^{-1}. The same experimental conditions were used for all samples. Surface damage induced by the laser was not observed, thus allowing for accurate measurements to be performed.

It is worth noting that the SEM, ED-XRD, EDS, and Raman spectroscopy measurements were accurately repeated for reproducibility. In particular, SEM/EDS data were collected on four (see SI) samples from four different pyrolysis experiments at 900 °C and we systematically observed the presence of Cu nano-roses; moreover, the ED-XRD measurements and Raman spectroscopy were iterated after a long period of time (months) to carefully observe the stability in air of elemental Cu against its oxidation.

3. Results and Discussion

The morphologies and structures of the pyrolyzed carbon powders were determined using HR-field emission scanning electron microscopy equipped with selected area electron energy dispersive X-ray spectroscopy.

The SEM images at 53.54 × 66.33 μm^2 and that of the overlapped false color table from EDS total yield spectra, taken with the Zeiss system FEG-SEM, LEO 1530 operating at an accelerating high voltage (HV) of 20.0 KV, are reported in Figure 1a,b.

At this magnification, the C powders display the coexistence of structures at various scales, from large flakes a few μm across to small spheres of some nanometres.

They are inconsistently arranged, even if somehow, they keep the memory of their original shape attributed to the bio-waste, [40], *Allium cepa*, L., [41] (onion vulgaris) peels from which they derive. On the other hand, Figure 1b evidences the different chemical composition, Na, O, Ca, Cl, K, Si, Al, and Mg, in addition to the predominant carbon, in close agreement with what reported in [40] and to the fact that the red onion vulgaris already contains these elements as precursors and, probably, in a conjugate form.

The false color EDS images of C (red), Ca (light blue), K (green), O (dark blue), Mg (magenta), and S (yellow) and their corresponding $K\alpha_1$ and $K\alpha_2$ shells are shown in Figure 1c–h, whereas Figure 1i shows the intensity of the $L\alpha_1$, $L\alpha_2$ and $K\alpha_1$, $K\alpha_2$ emission lines as a function of increasing energy for these elements. We can easily note, from the inset, that the presence of chemical species different from carbon can mainly be assigned to impurities, including the Cu $L\alpha_1$, $L\alpha_2$ emission lines that are clearly visible at around (0.93–0.95) KeV of energy, as well as the others $K\alpha_1$, $K\alpha_2$, and $K\alpha_3$ less intense around (8.0–8.9) KeV, proving C to be over 80%. The Si peak originated from the substrate.

A typical HR-SEM image, (58.56 × 77.91) μm^2, from C nanopowders supported on the gold substrate at magnifications of 3.54 K× and an electron acceleration HV of 2.0 KV, collected by using the Zeiss FE-SEM, is shown in Figure 2a. At first sight, we observe very defined and large C flakes (from 5 to 50 μm in length) randomly oriented and occupying most of the image area. Smaller structures scattered over the entire surface of these C flakes are clearly visible. Among these, three vaguely spherical objects (indicated with blue arrows) can be seen, the largest (red arrow) having a diameter of ~7 μm and the other smaller two of approximately 0.5 μm (yellow arrows). These particles were studied in a detailed morphological and chemical analysis, described hereafter.

Figure 2b–d show the SEM images at a higher resolution (17.92, 46.64, 169.32) K× of the largest spherical structure located at the center of the image of Figure 2a. We can interestingly remark the presence of rolled-up structures like nano-roses, distributed in a fractal like pseudo-morphism. The red dashed circle in Figure 2b with the diameter B = 2.63 μm indicates one of the composite structures that in a mathematical similarity forms the entire larger sphere of diameter A = 7.54 μm marked with a dashed light-blue circle. The yellow dashed circle with a diameter C = 0.92 μm emphasizes a single small rounded structure that builds-up the entire larger object in the dashed red circle.

Although in our bi-dimensional SEM images (consider for example the dotted light-blue area), we collapsed the three-dimensional reality of the rounded nano-roses on two-dimensional projections, we could extract some geometrical relations of the similarity among the spheres. One should also bear

in mind that the circles drawn in Figure 2b must be considered as an average. In particular, with the dotted light-blue circle we tried to enclose the maximum possible nanostructures.

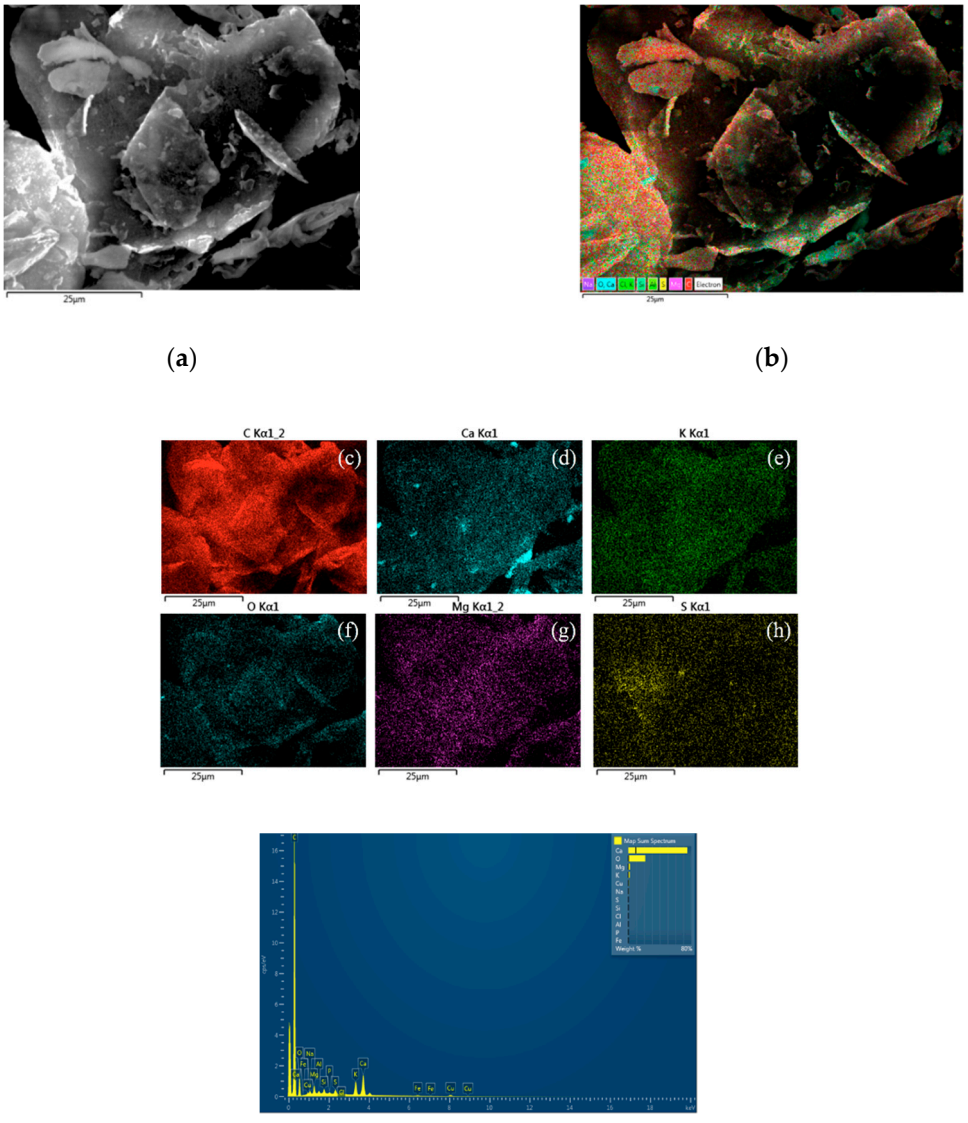

Figure 1. (**a**) SEM images at (53.54 × 66.33) μm^2 of carbon nanopowders, obtained by pyrolysis of *Allium cepa*, L., [41] and (**b**) false colors table from EDS total yield spectra; (**c**–**h**) separately false colors EDS images of C (red), Ca (light blue), K (green), O (dark blue), Mg (magenta), and S (yellow) and (**i**) the intensity of Lα_1, Lα_2 and Kα_1, Kα_2 emission lines, as a function of energy, of the elemental chemical impurities present in the C nanopowders.

Despite these simplifications, a close inspection of Figure 2 suggests some interesting points to consider: If we calculate the ratios between the diameters of the various circles, i.e., A:B and B:C, we get the same value of 2.86, which allows A:C to be expressed as about n times C, where n is an integer and is equal to 9. This means that the pseudo-fractal feature that is apparent at first visual inspection of the SEM images can be confirmed as a numerical relationship based on this simple geometric observation.

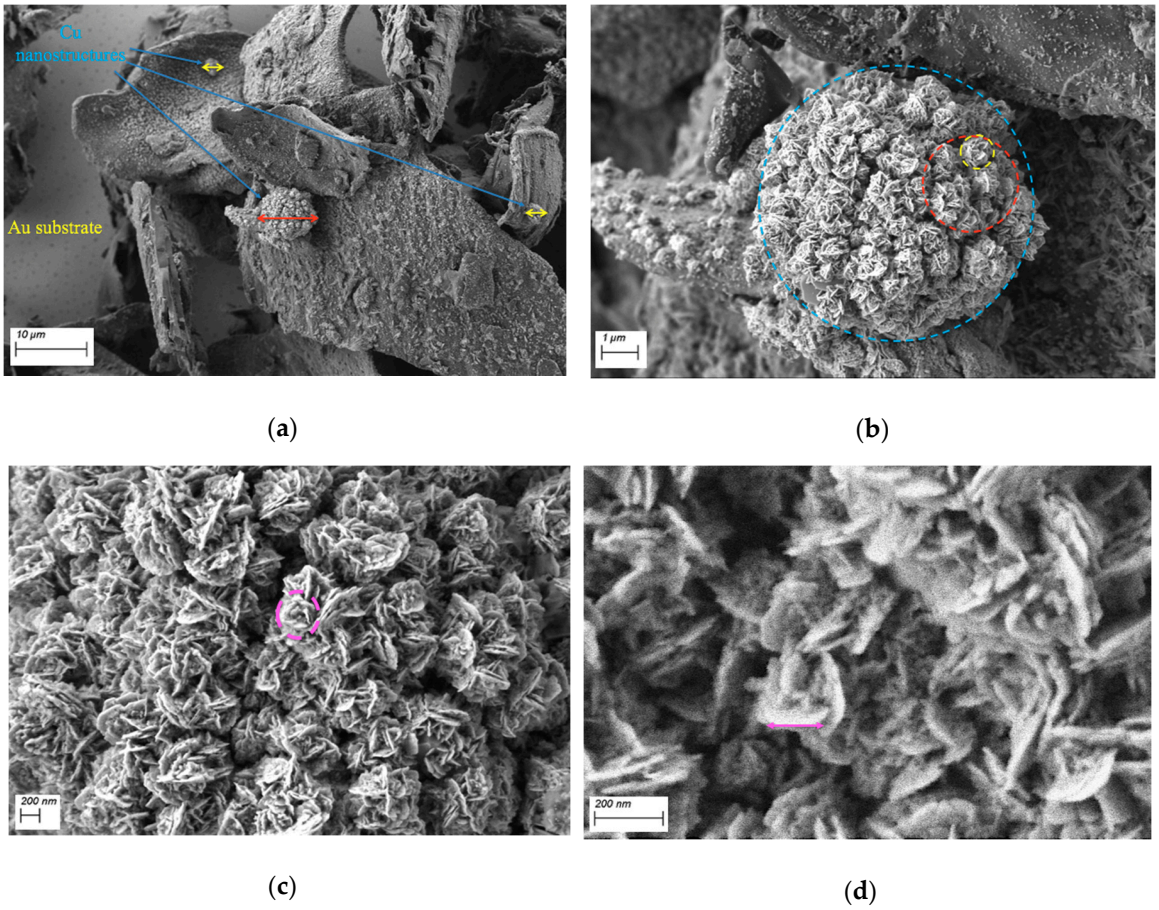

Figure 2. (**a**) High-resolution SEM image, (58.56 × 77.91) μm^2, from C nanopowders supported on gold substrate at a magnification of 3.54 K×; (**b**–**d**) SEM images at a higher resolution of (17.92, 46.64, 169.32) K× magnifications.

By increasing the magnification, as shown in Figure 2c, we can observe the petals of the individual nano-rose better, indicated, as a guide for the eyes, by the dashed pink circle. Each single petal (Figure 2d) has, on average, a lateral dimension of about 172 nm (pink arrow), with few larger or smaller petals.

Furthermore, it seems that the individual nano-rose (see those within the yellow and red circles in Figure 2b) uniformly covers a hypothetical sphere, the largest, as a spherical shell of a smaller inner diameter. We can imagine that the two structures of a smaller diameter indicated in Figure 2a by yellow arrows are also composed, in the same way, by nano-roses, considering that they are shown to be jagged in their external lines, having a similar gleaning profile. This is an additional intriguing aspect since it would suggest that these pseudo-fractal structures present on the external surface of the sphere also occur inside its volume, assuming a 3D fractal similitude, where the single nano-rose may be considered as the building block.

To identify the chemical composition of the nano-roses, we performed EDS microanalysis using the Bruker system. Figure 3a shows the SEM image that outlines the area where the EDS data were collected (3.8 K×, HV = 15 KV). Figure 3b–f display, respectively, the X-ray fluorescence maps for C, Ca, Mg, O, and Cu collected on the same area as in Figure 3a.

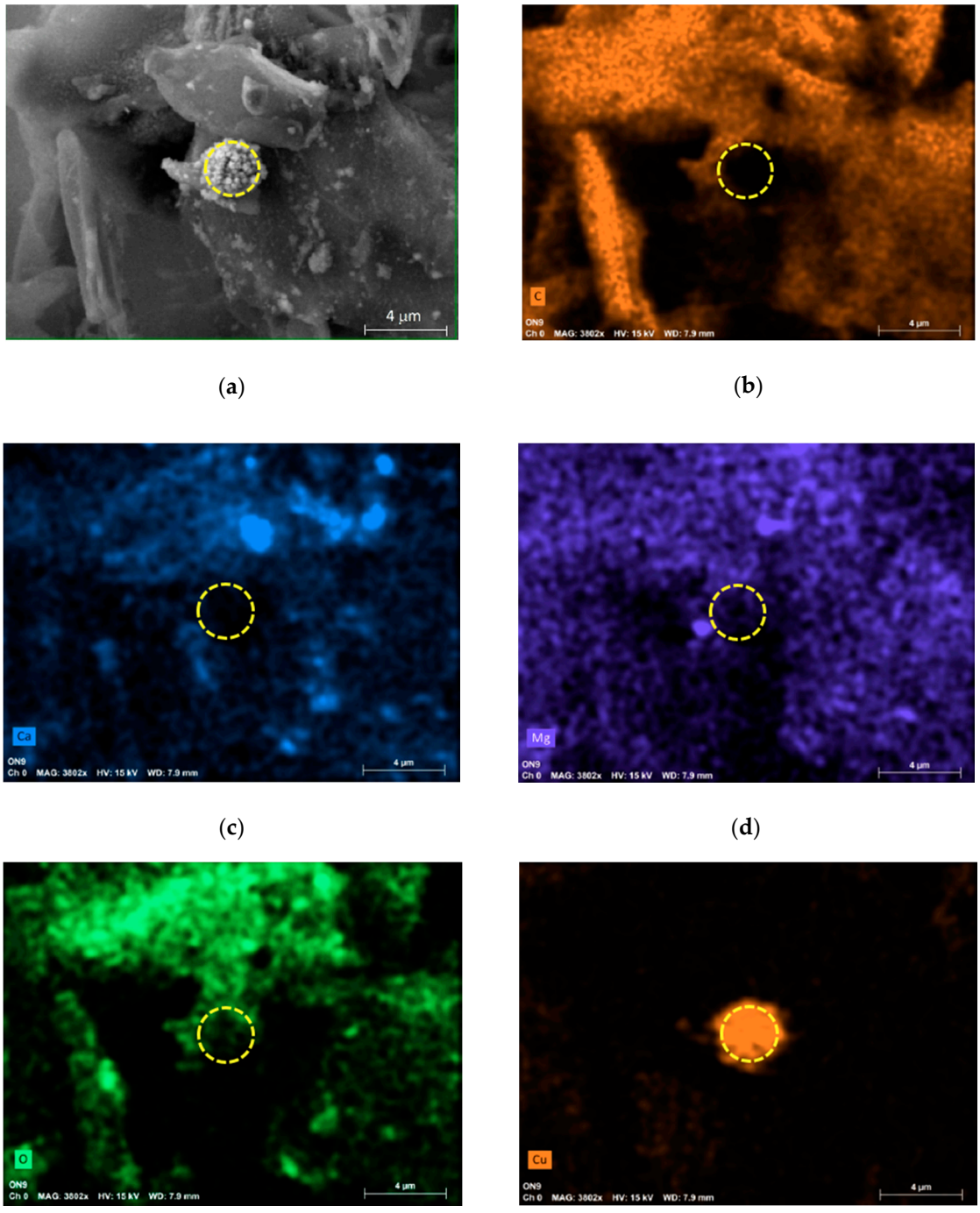

Figure 3. (**a**) SEM image (3.8 K×, HV = 15 KV) that outlines the area of the EDS measurements reported in (**b**–**f**). The dashed yellow circle, located in the same position in all images, is superimposed as an eye guide to delimit the nano-roses' structure.

Interestingly, we may observe from these elemental maps that the nano-roses are constituted of Cu, as shown in Figure 3f, and in particular by comparison of Figure 3e,f that are mainly composed of metallic Cu^0.

This represents a very intriguing point, since to date, no structures similar to our nano-roses have been described, considering both the morphology of the crystallites and their composition. Typically, the nanostructures of copper reported in the literature, which were mainly obtained from a liquid phase

by the immersion of pure copper sheets, have been found to be systematically composed of oxidized copper, CuO [17–25], showing nanostructures in the form of flowers but completely dissimilar from those reported in this paper [25]. The only exception is the Cu nanoflowers, constituted of metallic Cu^0 according to X-ray diffraction and X-ray spectroscopy measurements [43], obtained by a wet chemical process using $Cu[(acac)_2]$, acac = acetylacetonate as the reagent, oleyl amine both as the solvent and reducing agent, and cetyltrimethylammonium bromide as the capping agent.

We extrapolated that the main driving force used to obtain the Cu nano-roses from red onion peels is the high temperature applied during the annealing process performed in the inert nitrogen atmosphere. This produced both the expulsion of copper from its original organic molecules and the prevention of the oxidation onset to finally give rise to these particular Cu nanostructures. One cannot, however, exclude that the presence of elemental carbon may catalyze the Cu^0 nano-rose formation. In this respect, experiments are in progress to elucidate the actual mechanism of the formation of this new kind of Cu agglomeration, addressing both the physical and chemical aspects involved. This is a crucial point to clarify considering that both our results and those of [43] demonstrate that it is possible to obtain Cu^0 crystalline structures that are stable in air.

In the past, Ag structures have been obtained from the reaction of silver nitrate and ascorbic acid in an acidic aqueous solution of polynaphthalene [44]. Such structures are composed of metallic Ag^0 nanoparticles of about 10 nm in diameter linearly ordered inside a filamentous polymer sheath with a mesometric morphological structure in the flower form of about 10 microns in diameter, having meso-petals of a lanceolate shape. This constitutes an example where the Ag nanoparticles are kept chemically inert by a polymeric protective sheath that surrounds them. On the contrary, in the case of our copper nano-roses, as also reported in [43], the structures are self-protected against any oxidation or sulfurization, coming from air or from the precursors of the pyrolyzed carbon nanostructures.

To validate this result, the ED-XRD spectrum was collected on the carbon nanostructures as a function of the quantum momentum scattering parameter. In Figure 4, we can easily observe the presence of four peaks, two of which are assigned to the (002) and (101) reflections of the graphitic form of carbon indexed according to ICCD card number 00-001-0640 and corresponding to interplanar spacings with d = 3.380 Å and d = 2.020 Å, respectively; the other two are attributed to the (111) and (200) diffraction peaks of metallic copper [ICCD card number 00-001-1241] and are due to the interplanar spacings with d = 2.080 Å and d = 1.810 Å, respectively [21,24,25,43].

It is worth noting that the (110), (002), (-111), (111), and (200) diffraction peaks from CuO, which are expected in the region between 2.1 and 2.9 $Å^{-1}$ [21,24,25], are completely absent in Figure 4, confirming the EDS results. Indeed, the most intense reflection of CuO, (-111) at $2\theta = 35.744°$ (ICDD Reference code: 00-001-1117), would have been located at q = 2.50 $Å^{-1}$, and is clearly absent. Furthermore, the presence of crystalline CuS (ICDD Reference code: 00-07-0876) is also excluded: the main (103) reflection peak should have been located at q = 2.23 $Å^{-1}$ [45] and is missing in our pattern.

Finally, Figure 5 displays the Raman spectrum from the C nanostructures. Two main peaks labelled D and G, located at 1386 and 1587 cm^{-1}, are related to the E_{2g} in the plane vibrational mode of the hexagon atoms in the honeycomb C graphitic arrangement and to the defects peak [46–48].

The G-mode peak is found at 1587 cm^{-1}. Such a value, slightly blue-shifted with respect to highly crystalline graphite (G-mode at about 1580 cm^{-1}) [46–48], can be attributed to the nanometric-sized C-particles. This agrees with [46–48], where a frequency shift of about 15 cm^{-1} towards higher wavenumbers was found in some samples with extremely small graphite crystal sizes [46]. Several Raman spectra were collected on different portions/grains of the C nanostructures in order to obtain appreciable reproducibility. Notably, the presence of the main Raman features from CuO (295 cm^{-1}) [26] and CuS (473 cm^{-1}) [27–30] was never detected.

The red rectangle in Figure 5 delimits a region between 250 and 820 cm^{-1}, enlarged in the inset, which shows a flat area without features, where typically the structures of Cu oxides and sulphides are found [26–30]. This observation is in perfect agreement with all the described data, confirming that the

copper nano-roses exposed to air have the composition of metallic Cu^0 and thus are self-protected against oxidation from the external atmosphere.

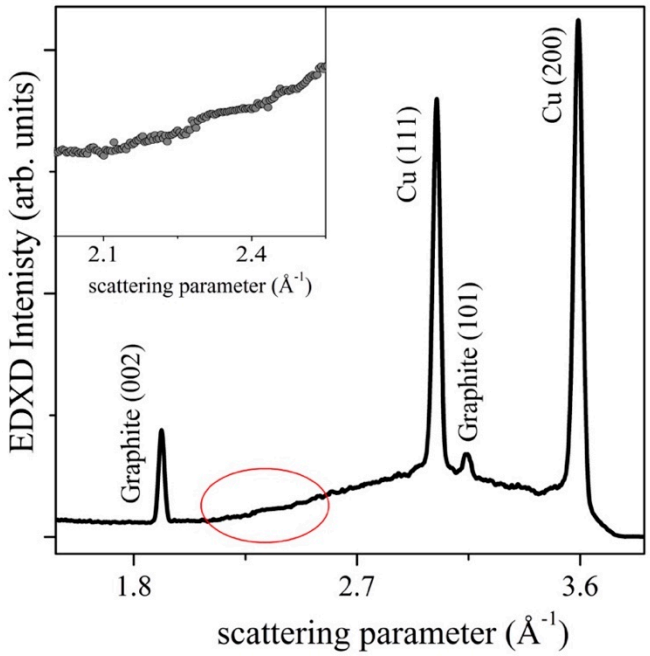

Figure 4. Selected energy dispersive XRD pattern collected upon carbon nanostructures, clearly indicating the presence of crystalline metallic Cu and graphite. The red circle evidences a region magnified in the inset, where the signature of crystalline CuO and CuS would be expected. No Bragg reflections related to those compounds are present.

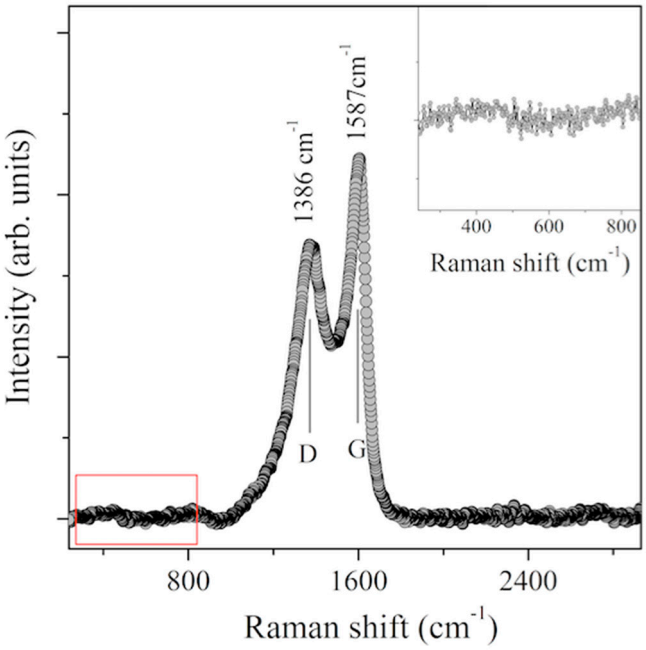

Figure 5. Raman spectrum from C nanostructures. In the inset, the region evidenced by the red rectangle is highlighted.

One hypothesis that could explain this important result lies in the possibility of interpreting the petals of the nano-roses as consisting of stacked layers of Cu [111] planes, such as [43], graphitic-like arranged, and thus resistant to possible oxidation.

4. Conclusions

Green carbon nanostructures produced by the bio-pyrolysis of *Allium cepa*, L., [41] from India [39,40] were studied through a combination of SEM/EDS, ED-XRD, and Raman spectroscopy, showing the self-assembly formation of metallic copper nanostructures. SEM images displayed for the first time the presence of rolled-up structures, called nano-roses for their evident shape, distributed in a fractal-like pseudo-morphism. The single nano-rose unit of 0.92 μm in diameter revealed rolled petals of nanometric size, with a lateral dimension of about 172 nm. The single nano-roses are arranged in ordered groups, occupying ideal circular structures of about 2.63 μm. These structures further unite to form a larger circle of 7.54 μm in diameter, exhibiting a quite uniform distribution, although this description represents a geometric simplification. The global ensemble of observed nano-roses indeed consists of spherical three-dimensional objects. EDS microanalysis showed that the nano-roses are constituted by metallic Cu^0, as confirmed by ED-XRD and Raman spectroscopy measurements. The data excluded the presence of copper oxides and/or copper sulphides.

Remarkably, in this work, the Cu nano-roses showed a morphology with an evidently increased surface/bulk ratio. This observation suggests, as also mentioned in [32] for protein–inorganic hybrid Cu^{2+} phosphate nanoflowers, the possibility of novel featured applications for these Cu nano-roses. These include (1) efficient electrodes in catalytic processes for fuel cells or (2) sensors for revealing the oxidation of fruits in the agri-food sector, thanks to their metallic unoxidized ground state. Indeed, in the particular conditions of a pH environment, the Cu^0 nano-roses can be oxidized, revealing the ripeness of the fruits, i.e., the enzymatic polyphenols to quinones' oxidation process.

Author Contributions: Conceptualization and methodology, P.D.P.; investigation and analysis, P.D.P., A.G., B.O., L.P., B.P.; data curation, P.D.P.; writing—original manuscript preparation—review and editing, P.D.P.; samples synthesis, S.S., G.H.; data discussion, P.D.P., A.G., B.O., L.P., B.P., L.S., F.D.P., G.D.V., C.O., C.Q., S.S., G.H. All authors have read and agreed with the published version of the manuscript.

Funding: This research received no external funding. G.D.V. was financially supported by MIUR-Italy "Dipartimenti di Eccellenza, ARTICOLO 1, COMMI 314–337 LEGGE 232/2016".

Acknowledgments: The authors have the pleasure to acknowledge Marco Guaragno for his invaluable technical support in XRD and Raman spectroscopy measurements and Federico Massimi for Zeiss FE-SEM data collection. G.H. would like to acknowledge the DST-Nanomission, Gov. of India for providing the grant N. SR/NM/NT-1026/2017.

Conflicts of Interest: The authors declare no conflict of interest.

References

1. Barth, J.V.; Costantini, G.; Kern, K. Engineering atomic and molecular nanostructures at surfaces. *Naure* **2005**, *437*, 671–679. [CrossRef] [PubMed]
2. Novoselov, K.S.; Geim, A.K.; Morozov, S.V.; Jiang, D.; Zhang, Y.; Dubonos, S.V.; Grigorieva, I.V.; Firsov, A.A. Electric Field Effect in Atomically, Thin Carbon Films. *Science* **2004**, *306*, 666–669. [CrossRef] [PubMed]
3. Vogt, P.; De Padova, P.; Quaresima, C.; Avila, J.; Frantzeskakis, E.; Asensio, M.C.; Resta, A.; Ealet, B.; Le Lay, G. Silicene: Compelling Experimental Evidence for Graphenelike Two-Dimensional Silicon. *Phys. Rev. Lett.* **2012**, *108*, 155501. [CrossRef] [PubMed]
4. Ezawa, M.; Salomon, E.; De Padova, P.; Solonenko, D.; Vogt, P.; Dávila, M.E.; Molle, A.; Angot, T.; Le Lay, G. Fundamental and functionalities of silicene, germanene and stanine. *La Rivista del Nuovo Cimento* **2018**, *41*, 175–224.
5. Li, X.; Ta, L.; Chen, Z.; Fang, H.; Li, X.; Wang, X.; Xu, J.-B.; Zhu, H. Graphene and related two-dimensional materials: Structure-property relationships for electronics and optoelectronics. *Appl. Phys. Rev.* **2017**, *4*, 021306. [CrossRef]
6. Bhimanapati, G.R.; Lin, Z.; Meunier, V.; Jung, J.; Cha, J.; Das, S.; Xiao, D.; Son, Y.; Strano, M.S.; Cooper, V.R.; et al. Recent Advances in Two-Dimensional Materials beyond Graphene. *ACS Nano* **2015**, *9*, 11509–11539. [CrossRef]
7. Geim, A.K.; Grigorieva, I.V. Van der Waals heterostructures. *Nature* **2013**, *499*, 419–425. [CrossRef]

8. Samadi, M.; Sarikhani, N.; Zirak, M.; Zhang, H.; Zhang, H.-L.; Moshfegh, A.Z. Group 6 transition metal dichalcogenide nanomaterials: Synthesis, applications and future perspectives. *Nanoscale Horiz.* **2018**, *3*, 90–204. [CrossRef]
9. Lee, M.M.; Teuscher, J.; Miyasaka, T.; Murakami, T.N.; Snaith, H.J. Efficient hybrid solar cells based on meso-superstructured organometal halide perovskites. *Science* **2012**, *338*, 643–647. [CrossRef]
10. Ham, S.; Choi, Y.-J.; Lee, J.-W.; Park, N.-G.; Kim, D. Impact of Excess CH_3NH_3I on Free Carrier Dynamics in High-Performance Nonstoichiometric Perovskites, Efficient Hybrid Solar Cells Based on Meso-Superstructured Organometal Halide Perovskites. *J. Phys. Chem.* **2017**, *121*, 3143–3148.
11. Liu, Y.; Ai, K.; Lu, L. Polydopamine and Its Derivative Materials: Synthesis and Promising Applications in Energy, Environmental, and Biomedical Fields. *Chem. Rev.* **2014**, *114*, 5057–5115. [CrossRef] [PubMed]
12. De Padova, P.; Quaresima, C.; Perfetti, P.; Olivieri, B.; Leandri, C.; Aufray, B.; Le Lay, G. Growth of straight, atomically perfect, highly metallic silicon nanowires with chiral asymmetry. *Nano Lett.* **2008**, *8*, 271–275. [CrossRef] [PubMed]
13. De Padova, P.; Perfetti, P.; Olivieri, B.; Quaresima, C.; Ottaviani, C.; Le Lay, G. 1D graphene-like silicon systems: Silicene nano-ribbons. *J. Phys. Condens. Matt.* **2012**, *24*, 223001. [CrossRef] [PubMed]
14. De Padova, P.; Kubo, O.; Olivieri, B.; Quaresima, C.; Nakayama, T.; Aono, M.; Le Lay, G. Multilayer Silicene nanoribbons. *Nano Lett.* **2012**, *12*, 5500–5503. [CrossRef] [PubMed]
15. Ertl, G. Reactions at Surfaces: From Atoms to Complexity (Nobel Lecture). *Angew. Chem. Int. Ed.* **2008**, *47*, 3524–3535. [CrossRef]
16. Hoffmann, R. Small but Strong Lessons from Chemistry for Nanoscience. *Angew. Chem. Int. Ed.* **2013**, *52*, 93–103. [CrossRef]
17. Poreddy, R.; Engelbrektb, C.; Riisager, A. Copper oxide as efficient catalyst for oxidative dehydrogenation of alcohols with air. *Catal. Sci. Technol.* **2015**, *5*, 2467–2477. [CrossRef]
18. Kidowaki, H.; Oku, T.; Akiyama, T.; Suzuki, A.; Jeyadevan, B.; Cuya, J. Fabrication and Characterization of CuO-based Solar Cells. *J. Mat. Sci. Res.* **2012**, *1*, 138–143. [CrossRef]
19. Al-Mayalee, K.H.; Saadi, N.; Badradeen, E.; Watanabe, F.; Karabaca, T. Optical and Photoconductive Response of CuO Nanostructures Grown by a Simple Hot-Water Treatment Method. *J. Phys. Chem. C* **2018**, *122*, 23312–23320. [CrossRef]
20. Hsieh, C.-T.; Chen, J.-M.; Lin, H.-H.; Shih, H.-C. Field emission from various CuO nanostructures. *Appl. Phys. Lett.* **2003**, *83*, 338–3385. [CrossRef]
21. Liu, J.; Huang, X.; Li, Y.; Sulieman, K.M.; Heb, X.; Sun, F. Hierarchical nanostructures of cupric oxide on a copper substrate: Controllable morphology and wettability. *J. Mater. Chem.* **2006**, *16*, 4427–4434. [CrossRef]
22. Zhang, W.; Ding, S.; Yang, Z.; Liu, A.; Qian, Y.; Tang, S.; Yang, S. Growth of novel nanostructured copper oxide (CuO) films on copper foil. *J. Crys. Growth* **2006**, *291*, 479–484. [CrossRef]
23. Liu, Y.; Chu, Y.; Zhuo, Y.; Li, M.; Li, L.; Dong, L. Anion-Controlled Construction of CuO Honeycombs and Flowerlike Assemblies on Copper Foils. *Growth Des.* **2007**, *7*, 467–470. [CrossRef]
24. Song, M.-J.; Hwang, S.W.; Whang, D. Non-enzymatic electrochemical CuO nanoflowers sensor for hydrogen peroxide detection. *Talanta* **2010**, *80*, 1648–1652. [CrossRef]
25. Gao, P.; Liu, D. Facile synthesis of copper oxide nanostructures and their application in non-enzymatic hydrogen peroxide sensing. *Sens. Actuators B* **2015**, *208*, 346–354. [CrossRef]
26. Xu, J.F.; Ji, W.; Shen, Z.X.; Li, W.S.; Tang, S.H.X.; Ye, R.; Jia, D.Z.; Xin, X.Q. Raman Spectra of CuO Nanocrystals. *J. Raman Spectrosc.* **1999**, *30*, 413–415. [CrossRef]
27. Phuruangrat, A.; Thoonchalong, P.; Thongtem, S.; Thongtem, T. Synthesis of CuS with different morphologies by refluxing method: Nanoparticles in clusters and nanoflakes in spongelike clusters. *Chalcog. Lett.* **2012**, *9*, 421–426.
28. Phuruangrat, A.; Thongtem, T.; Thongtem, S. Characterization of copper sulfide hexananoplates, and nanoparticles synthesized by a sonochemical method. *Chalcog. Lett.* **2011**, *8*, 291–295.
29. Thongtem, T.; Phuruangrat, A.; Thongtem, S. Characterization of copper sulfide nanostructured spheres and nanotubes synthesized by microwave-assisted solvothermal method. *Mat. Lett.* **2010**, *64*, 136–139. [CrossRef]
30. Thongtem, T.; Phuruangrat, A.; Thongtem, S. Formation of CuS with flower-like, hollow spherical, and tubular structures using the solvothermal-microwave process. *Curr. Appl. Phys.* **2009**, *9*, 195–200. [CrossRef]
31. Wang, Z.; Zhang, X.; Zhang, Y.; Li, M.; Qin, C.; Bakenov, Z. Chemical Dealloying Synthesis of CuS Nanowire-on-Nanoplate Network as Anode Materials for Li-Ion Batteries. *Metals* **2018**, *8*, 252. [CrossRef]

32. Ge, J.; Lei, J.; Zare, R.N. Protein–inorganic hybrid nanoflowers. *Nat. Nanotechnol.* **2012**, *7*, 429–432. [CrossRef] [PubMed]
33. Kroto, H.W.; Heat, J.R.; O'Brien, S.C.; Curl, R.F.; Smalley, R.E. C_{60}: Buckminsterfullerene. *Nature* **1985**, *318*, 162–163. [CrossRef]
34. Taylor, R.; Hare, J.P.; Abdul-Sada, A.K.; Kroto, H.W. Isolation, Separation and Characterisation of the Fullerenes C_{60} and C_{70}: The Third Form of Carbon. *J. Chem. Soc. Chem. Commun.* **1990**, 1423–1425. [CrossRef]
35. Ettl, R.; Chao, I.; Diederich, F.; Whetten, R.L. Isolation of C_{76}, a chiral (D2) allotrope of carbon. *Nature* **1991**, *353*, 149–153. [CrossRef]
36. Sun, G.; Kertesz, M. Theoretical 13C NMR Spectra of IPR Isomers of Fullerenes C_{60}, C_{70}, C_{72}, C_{74}, C_{76}, and C_{78} Studied by Density Functional Theory. *J. Phys. Chem. A* **2000**, *104*, 7398–7403. [CrossRef]
37. Dekker, C. Carbon nanotubes as molecular quantum wires. *Phys. Today* **1999**, *52*, 22–28. [CrossRef]
38. Geim, A.K.; Novoselov, K.S. The rise of graphene. *Nat. Mater.* **2007**, *6*, 183–191. [CrossRef]
39. Kharisu, C.S.; Koki, I.B.; Ikram, R.; Low, K.H. Elemental variations and safety assessment of commercial onions (*Allium cepa*) by inductively coupled plasma-mass spectrometry and chemometrics. *Int. Food Res. J.* **2019**, *26*, 1717–1724.
40. Supriya, S.; Sriram, G.; Ngaini, Z.; Kavitha, C.; Kurkuri, M.; De Padova, I.P.; Hegde, G. The Role of Temperature on Physical–Chemical Properties of Green Synthesized Porous Carbon Nanoparticles. *Waste Biomass Valor.* **2019**. [CrossRef]
41. Linnaei, C. *Species Plantarum*; Holmiae Impensis Laurentii Salvii: Uppsala, Sweden; Paris, France, 1753; Volume Tomus I, pp. 300–301.
42. Paci, B.; Generosi, A.; Rossi Albertini, V.; Agostinelli, E.; Varvaro, G.; Fiorani, D. Structural and Morphological Characterization by Energy Dispersive X-ray Diffractometry and Reflectometry Measurements of Cr/Pt Bilayer Films. *Chem. Mater.* **2004**, *16*, 292–298. [CrossRef]
43. Li, Z.; Ma, Z.; Wen, Y.; Ren, Y.; Wei, Z.; Xing, X.; Sun, H.; Zhang, Y.-W.; Song, W. Copper Nanoflower Assembled by Sub-2 nm Rough Nanowires for Efficient Oxygen Reduction Reaction: High Stability and Poison Resistance and Density Functional Calculations. *ACS Appl. Mater. Interfaces* **2018**, *10*, 26233–26240. [CrossRef] [PubMed]
44. Suber, L.; Plunkett, W.R. Formation mechanism of silver nanoparticle 1D microstructures and their hierarchical assembly into 3D superstructures. *Nanoscale* **2010**, *2*, 128–133. [CrossRef] [PubMed]
45. Takéuchi, Y.; Kudoh, Y.; Sato, G. The crystal structure of covellite CuS under high pressure Up to 33 kbar. *Zeitschrift für Kristallographie* **1985**, *173*, 119–128. [CrossRef]
46. Tuinstra, F.; Koenig, J.L. Raman Spectrum of Graphite. *J. Chem. Phys.* **1970**, *53*, 1126–1130. [CrossRef]
47. Puech, P.; Kandara, M.; Paredes, G.; Moulin, L.; Elsa Weiss-Hortala, E.; Kundu, A.; Ratel-Ramond, N.; Plewa, J.-M.; Pellenq, R.; Monthioux, M. Analyzing the Raman Spectra of Graphenic Carbon Materials from Kerogens to Nanotubes: What Type of Information Can Be Extracted from Defect Bands? *C* **2019**, *5*, 69. [CrossRef]
48. Ferrari, A.C.; Meyer, J.C.; Scardaci, V.; Casiraghi, C.; Lazzeri, M.; Mauri, F.; Piscanec, S.; Jiang, D.; Novoselov, K.S.; Roth, S.; et al. Raman Spectrum of Graphene and Graphene Layers. *Phys. Rev. Lett.* **2006**, *97*, 187401. [CrossRef]